IMPROVING THE OPERATING COMFORT OF THE ELECTRIC MINI-TILLER BASED ON SIMULATION ANALYSIS AND FIELD TEST
/
基于仿真分析和田间试验的电动微耕机操作舒适性提高

Po Niu, *Jian* Chen, *Chenjun* Hu, *Jindou* Zhao
Southwest University, College of Engineering and Technology/P.R China
Tel:8613628384705; E-mail: jianchen@swu.edu.cn
DOI*: https://doi.org/10.35633/inmateh-60-25*

ABSTRACT

Now the engine mini-tiller has become indispensable agricultural machinery in vast hilly and mountainous areas of Southwest China. Many researches have been made to improve its operating comfort, but little effects have been obtained. As an alternative, a new type of electric mini-tiller was developed. For further improvement of its operating comfort, simulation analysis and field test were integrated to decrease the vertical force and vibration RMS values at the handle. The results showed that when the position of centre of gravity moved 19.78 cm, the vertical force was reduced from 154.24 N to 0 N, and vibration RMS values decreased by 20.16% under working condition.

摘要

目前，微耕机已经成为中国西南广大丘陵山区不可缺少的农业机械。为了改善其操作舒适性，做了许多研究，但是效果很小。因此，开发了一种新型电动微耕机，为了进一步改善其操作舒适性，采用仿真分析和田间试验相结合的方法来减小扶手处的垂向力和振动加速度值。结果表明，在正常工作条件下，当重心位置移动 19.78 cm 时，垂向力由 154.24 N 减小到 0 N，振动加速度值减小 20.16％。

INTRODUCTION

Being small volume, light weight, simple structure and easy transfer in the farm land, the internal combustion engine mini-tiller has become the main and indispensable agricultural machinery in the hilly and mountainous area of Southwest China *(Chen J. et al, 2014)*. However, there have been urgent needs of improvement of its operating comfort, especially nowadays, for most tiller operators are women and aging people in the area.

The mini-tiller is a kind of walking machinery and its operating comfort mainly relies on the vibration acceleration and the force applied to the operator's two hands through the tiller's handles. Therefore, decreasing the both can make the operating comfort increase.

The tiller's engine vibration is mainly caused by two coupling effects of cycling movement of the piston-connecting rod of the engine and periodical rotary blades cutting soils. The vibration acceleration at the handle can be reduced from two aspects: reducing vibration or obstructing vibration transmission from its resources to the operator's hands *(Ying Y.B. et al, 1994; Ragni L, 1999; Dong X.Q. et al, 2012; Xu L.Z. et al, 2014)*. *Bini* and *Kathirvel* deals with machine vibration, hand transmitted vibration of walking and riding type power tillers during rototilling in untilled and tilled fields and in transport mode on farm and bitumen roads. The results indicate that machine vibration increased with the increase in engine speed and major excitation of the power tiller vibration was the unbalanced inertial force of the engine *(Bini and Kathirvel, 2006)*. *Tewari* and *Dewangan* pointed that the operators of hand tractors experience high levels of vibration in the hand and arm, which cause early fatigue and result in shorter working hours. Suitable isolators were designed and installed in different strategic locations in the hand tractor in order to reduce the effect of vibration level, and hence reduce work stress. The results indicated that the engine mounting and the handle isolators reduced the vibration acceleration by more than 50% *(Tewari and Dewangan, 2009)*. *Liang Xincheng et al*. selected 1Z-105 diesel mini tiller as a prototype, its vibration characteristics were analysed in the time and frequency domains and the effects on the human body were explored, and suggestion was made regarding the handling comfort of the mini tiller *(Liang X.C. et al, 2018)*. But these researches have little effect; the main reasons lie in implementation of measures stated above being difficult without a substantial increase in size, weight and price of the tiller *(Thomas H.L. et al, 2015; Caffaro F. et al, 2016; Niu P. et al, 2017)*, which is unacceptable for local the farmers.

As a countermeasure, a new type of electric mini-tiller was developed, which can achieve a tillage depth of 10 cm or more and replace the engine tiller for farming operations in dry land tillage and land preparation in vast hilly and mountainous areas of Southwest China. Because its power is a group of lithium battery and a brushless DC motor instead of combustion engine, its vibration resulting from the power is decreased, but the vibration caused by periodical rotary blades cutting soils still exists, further efforts are needed. Until now, vibration of electric mini-tillers has not captured much researchers' attentions, perhaps because unlike the one mentioned above, the majority of existing ones were only suitable for shallow tillage, in other words, they can get a tillage depth of about 5 cm *(Cai K. et al, 2013; Gao H.S. et al, 2012; Zhao R.H. et al, 2015)*. Therefore, vibration produced by these kinds of electric mini-tillers is not so intense.

The other factor that influences tiller's operating comfort is the force applied to operator's hands. It can be decomposed into three components along three directions, namely, top-bottom, left-right and front-back. Under normal circumstances, the latter two components are small and uncontrollable compared with the first one *(Hu C.J., 2018)*. So, the component of the force in the direction top-bottom, i.e. the vertical force should be carefully considered to increase the operating comfort. When cultivating clay soil, a certain vertical force is necessary to ensure adequate tillage depth. However, under some soil conditions, a small force is sufficient. Therefore, the determination of the best vertical force for different soils is a problem worth exploring, but so far there are few reports about it.

In this study, the newly developed electric mini-tiller mentioned above was taken as the research object, the method of combining three-dimensional modelling, force analysis, simulation analysis and field test was adopted to decrease its vibration and vertical force at the handles and improve its operating comfort by changing the position of the tiller centre of gravity, so as to provide available theory and reference to improve the operating comfort of tillers.

MATERIALS AND METHODS
Electric mini-tiller

The electric mini-tiller is mainly composed of handrail, motor controller, electric motor (brushless DC motor, rated power, 0.75 kW), battery pack (60V20Ah lithium battery), rotary blade roller (type of blade, machete; no. of blades, 4×3), transmission system (direct drive), frame, and depth-limiting device, as shown in fig.1. The transmission system consists of power input shaft, one pair of straight bevel gears and power output shaft. The significant parameters of the tiller are listed in table 1, and the material properties of its primary components are delineated in table 2.
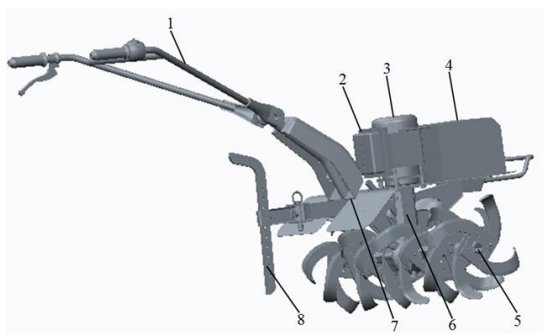
Fig. 1 - Electric mini-tiller
1 – Handrail; 2 – Motor controller; 3 – Electric motor; 4 – Battery pack; 5 – Rotary blade roller;
6 – Transmission system; 7 – Frame; 8 – Depth limiting device

Table 1

Parameters

Item	Mass	Tillage width	Tillage depth	Forward speeds		
				Slow	Medium	Rapid
	[kg]	[cm]	[cm]	[m/s]	[m/s]	[m/s]
Parameter	50	70	≥10	0.1(only used for field transfer)	0.3 (mainly used for field transfer, rarely for tilling)	0.5 (used for tilling)

Table 2

Material parameters

Component	Handrail	Frame	Gearbox housing	Power input/output shaft	Straight bevel gear	Rotary blade shaft	Rotary blade
Material	E235B (ISO 630)	E235B (ISO 630)	Cr20 (ISO/R 185)	18CrMo4 (ISO 683)	18CrMo4 (ISO 683)	18CrMo4 (ISO 683)	Type SC; Type DC (ISO 630)
Density [g/cm³]	7.85	7.85	7.00	7.86	7.86	7.86	7.82

Because the electric motor and battery pack consist of many kinds of materials, their densities were obtained by measuring their mass and volume and then performing a simple calculation. The results were 2.14 g/cm³ and 8.90 g/cm³, respectively.

Test instruments and software

The key performance indices of SC900 soil firmness tester (Spectrum Technologies, Inc., United States, fig.2 [a]), 356A16 three-dimensional acceleration sensor (PCB Piezotronics, Inc., United States, fig.2 [b]), and LMS SCADAS Mobile (Siemens, Germany, fig.2 [c]) are listed in table 3-table 5.

[a] SC900 soil firmness tester   *[b] Three-dimensional acceleration sensor*   *[c] LMS SCADAS Mobile*

Fig. 2 - Test instruments

Table 3

Key performance indices of SC900 soil firmness tester

Index	Pressure range	Depth range	Resolution	Depth precision
	[kPa]	**[mm]**	**[kPa]**	**[mm]**
Index	0–7000	0–450	35	12.5

Table 4

Key performance indices of 356A16 three-dimensional acceleration sensor

Index	Range	Frequency	Transverse sensitivity	Mass	Sensitivity		
					X	*Y*	*Z*
	[g]	**[kHz]**	**[%]**	**[g]**	**[mV/g]**	**[mV/g]**	**[mV/g]**
Index	±50	0.3–6	<5	7.4	96.1	98.6	100.4

Table 5

Key performance indices of LMS SCADAS Mobile

Index	Dynamic range	Operation temperature	Input voltage	Digital signal rate
	[dB]	**[°C]**	**[V]**	**[kHz]**
Index	150	-20–50	±10	51.2

The LMS Test.Lab (LMS International NV, Belgium, fig.3) was used as the analysis software for the field testing of the tiller, mainly for vibration signal acquisition, processing, and analysis.
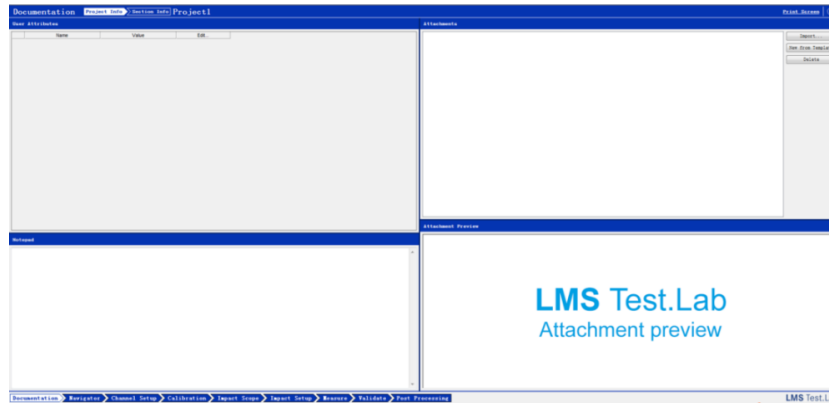
Fig. 3 - LMS Test.Lab

In the field test, the sampling frequency was set to 2 kHz and the Hann window was selected as the window function of the system.

Soil parameters

Five soil samples of the test farm plot were collected using a cutting ring. The soil moisture rate *c* was calculated using equation (1):

$$c = \frac{m_a - m_b}{m_a} \cdot 100\% \quad [\%]$$ (1)

Where:

m_a is the soil sample mass before drying, g; and m_b is the soil sample mass after drying, [g].

The soil sample mass before and after drying, as well as the moisture rate, are listed in table 6.

Table 6

Soil moisture rate

Soil sample mass before drying	Soil sample mass after drying	Moisture rate	Average value
[g]	[g]	[%]	[%]
98.9665	80.8651	18.29	
92.0825	74.1260	19.50	
98.1202	82.6903	15.72	18.89
105.3226	84.4531	19.81	
106.3432	83.5563	21.14	

The soil density *ρ* can be calculated using equation (2):

$$\rho = \frac{m_a}{v} \quad [g/cm^3]$$ (2)

Where:

v is the soil sample volume, [cm^3].

The soil density values are listed in table 7.

Table 7

Soil density

Soil sample mass before drying	Soil sample volume	Soil density	Average value
[g]	[cm^3]	[g/cm^3]	[g/cm^3]
98.9665	59.41	1.96	
92.0825	59.41	1.54	
98.1202	59.41	1.65	1.74
105.3226	59.41	1.77	
106.3432	59.41	1.79	

When measuring the soil firmness, an SC900 soil firmness tester was inserted into the soil at a uniform speed (< 25 mm/s) in the vertical direction, and the soil firmness data were recorded once every 25 mm. The soil firmness values are listed in table 8.

Table 8

Soil firmness

Soil depths [mm]	0–50	50–100	100–150
Parameter value [kPa]	0–0.165	0.165–0.355	0.355–0.480

Methods

Fig.4 illustrates the research procedure. First, a three-dimensional model of the tiller was established and its centre of gravity determined using Creo/E software (Parametric Technology Corp., United States). The relationship between the centre of gravity position and the vertical force at the handles was determined using force analysis. Then, based on the relationship of the installation position and force among each part of the tiller, the vibration dynamic model and its balance equation were developed. The vibration simulation program of the electric mini-tiller-soil system was created based on the balance equation using MATLAB/Simulink software (MathWorks, Inc., United States). The vibration acceleration values at the handles obtained by the simulation analysis were then compared with those from the field test, so as to confirm whether three-dimensional modeling and simulation analysis could be used to analyse and improve the operating comfort of the electric mini-tiller. Finally, the centre of gravity position was adjusted by shifting the position of the battery pack, in order to reduce the vertical force at the handles to its minimum value of 0 N. The three-dimensional model and the vibration dynamic model of the tiller after the centre of gravity adjustment were developed, and the vibration acceleration values at the handles were obtained from the simulation analysis, which were then compared with those determined before the centre of gravity adjustment.
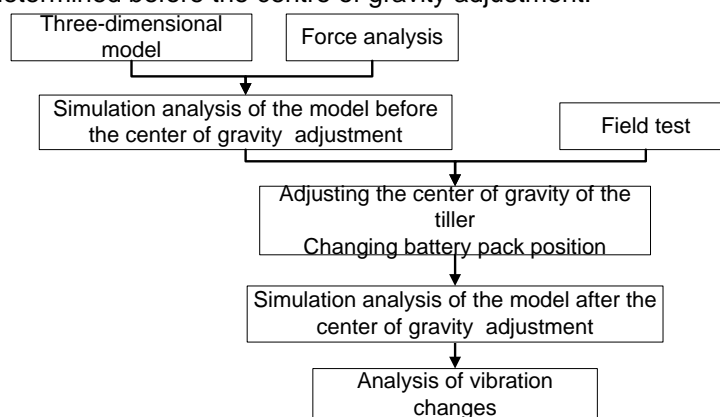
Fig. 4 - Research procedure

Field test

The test was conducted from 9:00 a.m. to 4:00 p.m. on December 19, 2018 on a farm plot (sandy loam), with a length of 50 m and a width of 35 m, located in the Hechuan District, Chongqing, China (29°39′45″ N, 106°23′45″ E; 210 m above mean sea level).

The three-dimensional acceleration sensor was fixed on the handle, according to ISO 5349-a. The *X*, *Y*, and *Z* directions of the sensor correspond to the vertical, forward-and-reverse, and left-to-right directions, respectively (fig.5). The field test is shown in fig.6; the tiller was progressing at a forward speed of 0.5 m/s.

Fig. 5 - Corresponding relation of *X, Y,* and *Z* directions   **Fig. 6 - Field test**

Mini-tiller vibration is a type of random vibration and can be described using statistical characteristic values. This study compared vibration acceleration values via the root mean square (RMS) values. The RMS values in the vertical direction (*X* direction) were selected as the research object, since vertical vibrations have the greatest impact on operating comfort *(Li G., et al, 2016; Hu C.J., 2018)*.

The vibration acceleration signals obtained from the field test were processed using LMS Test.Lab Signature Acquisition software. The vibration acceleration curve and the RMS values were then determined.

Determination of the centre of gravity of the three-dimensional model

Three-dimensional models of the main components of the tiller were established based on prototype size. Their masses were attained by defining the material parameters (table 2) of the models, and were then compared with the corresponding measured values of the prototype, as shown in table 9.

Table 9

Comparison of the masses of the three-dimensional model components with those of the prototype

Component	Mass of model [kg]	Mass of prototype [kg]	Relative error [%]
Handrail	3.21	3.27	1.87
Frame	13.32	13.56	1.80
Electric motor	6.59	6.68	1.37
Battery pack	8.38	8.52	1.67
Gearbox housing	4.78	4.85	1.46
Power input shaft	0.28	0.28	0
Power output shaft	0.36	0.36	0
Rotary blade shaft	0.95	0.96	1.05
Single rotary blade	0.44	0.44	0
Rotary blade roller	12.44	12.48	0.32

As can be seen from table 9, the model masses of the main components were in good agreement with those of the prototype, with all of the relative errors < 2.0%. Therefore, the three-dimensional model of the tiller was obtained by assembling the main model components in terms of their assembly relationship (fig.7). The total model mass was 49.36 kg, exhibiting a relative error of 0.13% compared with the prototype mass of 50 kg.

Fig. 7 - Three-dimensional model of the electric mini-tiller

As shown in fig.7, the coordinate system was established, with point O (the intersection point of the centre line of the power input shaft and the centre line of the power output shaft) as the origin, and the *X*, *Y*, and *Z* directions of the sensor corresponding to the forward-and-reverse, vertical, and left-to-right directions, respectively. Point C (-3.52 cm, 20.616 cm, and -0.042 cm), the centre of gravity of the three-dimensional model, was determined using Creo/E software.

Relationship between the centre of gravity and the vertical force at the handles

The force diagram of the rotary blade roller tilling soil is illustrated in fig.8. The angle β between OA and OC is 20° and the radius of the resultant force *R'* is 0.9 *R (Asl and Singh, 2009)*.
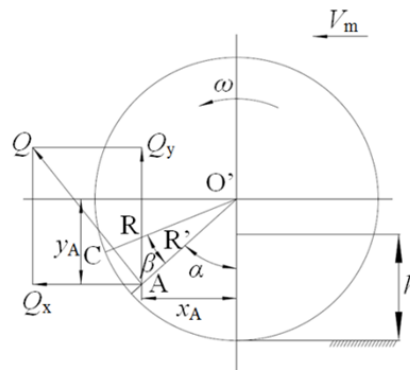
Fig. 8 - Force diagram of the rotary blade roller

Where:

R is the turning radius of the rotary blade roller, 160 mm; Q is the cutting resistance; Q_x and Q_y are the horizontal component force and vertical component force, [N] respectively; point A is the action point; and x_A and x_B are the horizontal distance and vertical distance, respectively, [cm].

From fig.8, the geometric relationship of the parameters is shown in equation (3):

$$\begin{cases} \alpha = \cos^{-1}\left[(R-h)/R\right] - 20° \\ Q_x = Q\cos\alpha \\ Q_y = Q\sin\alpha \\ x_A = R'\sin\alpha \\ y_A = R'\cos\alpha \end{cases} \tag{3}$$

Where:

Q can be calculated from $Q = T/R'$; T is the torque of rotary blade roller, and it can be calculated from $T = 9550\,P/n$; P is the power of the rotary blade roller, which is calculated from $P = P_n \cdot \eta_T$ (P_n is the rated power, 0.75 kW and η_T is the transmission efficiency, 0.97); n is the rotational speed of the rotary blade roller, 145 r/min; and h is the tillage depth, 10 cm.

According to Eq. (3), $\alpha = 48°$, $Q = 331$ N, $Q_x = 221$ N, $Q_y = 246$ N, $x_A = 10.7$ cm, and $y_A = 9.6$ cm.

When the electric tiller was progressing at a forward speed of 0.5 m/s, the coordinate system was established consistent with fig.7. The forces on each part of the tiller are shown in fig.9.
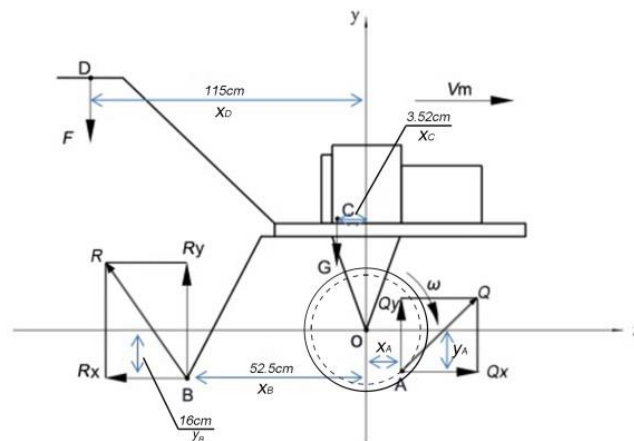

Fig. 9 - Force analysis of the electric mini-tiller

Where:

G is the gravity of the electric mini-tiller, $G = mg$, 484 [N]; U is the soil reaction force received by the depth-limiting device; U_x and U_y are the horizontal component force and vertical component force, respectively, [N]; point B is the action point; x_B and y_B are the horizontal distance and vertical distance, respectively, [cm]; C is the centre of gravity of the tiller; x_C is the horizontal distance, [cm]; F is the vertical force at the handles,

[N]; D is the action point; x_D is the horizontal distance, [cm]; and v_m is the tiller's forward speed, 0.5 m/s. The respective measured values of x_A, x_B, x_C, and x_D were 52.5 cm, 16 cm, 3.52 cm, and 115 cm.

Equation (4) can be obtained from the force balance:

$$\begin{cases} Q_y + U_y - F - G = 0 \\ Q_y x_A + Q_x y_A + G x_C + F x_D - U_x y_B - U_y x_B = 0 \\ Q_x - U_x = 0 \end{cases} \qquad (4)$$

When the acquired data (G, Q_x, Q_y, x_A, y_A, x_B and x_D) were input into equation (4), the relationship between F and x_C could be calculated:

$$7.744 x_C + F = 180.44 \qquad (5)$$

Before the centre of gravity adjustment, x_C was 3.52 cm and F was 154.24 N.

Simulation analysis

Since the deformations of the handrail, battery pack, electric motor, frame, and rotary blade roller can be neglected during the tilling process, their three-dimensional models can be simplified as rigid bodies, and the dynamic transmission process of the tiller can be simplified as a spring system without damping mass.

In addition, since the rotational speed of the rotary blade roller during the tilling process was relatively low, and the fluctuation of the cutting resistance was small, the cutting resistance can be simplified as a vertical constant force, allowing the dynamic interaction process between the rotary blade roller and the soil to be simplified as a forced vibration of a single-degree-of-freedom mass-spring-damper.

The construction of the vibration dynamic model of the tiller took into consideration the relationship of the installation position and force among each part (fig.9), as shown in fig.10.
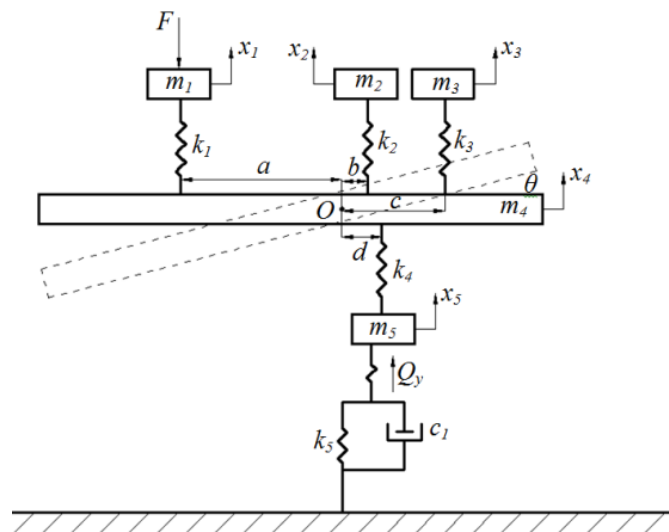
Fig. 10 - Vibration dynamic model

Where:

m_1, m_2, m_3, m_4, and m_5 are the masses of the handrail, electric motor, battery pack, frame, and rotary blade roller, respectively, [kg]; x_1, x_2, x_3, x_4, and x_5 are the vertical displacements of the centroid of the handrail, electric motor, battery pack, frame, and rotary blade roller, respectively, [cm]; k_1, k_2, k_3, and k_4 are the structural stiffness values between the frame and the handrail, electric motor, battery pack, and frame, respectively, 5.5 × 10⁷ N/m; k_5 is the soil equivalent stiffness, 4.5 × 10⁶ N/m; O is the centroid of frame; θ is the maximum pitch angle (the frame moving around its centroid), 0.03 rad; c_1 is the soil equivalent damping, 4.5 × 10³ N·s/m; a, b, c, and d are the horizontal distances from the action point of the handrail, electric motor, battery pack, and rotary blade roller to point O, which can be obtained by measuring, m; F is the vertical force at the handles, 152.24 N; and Q_y is the vertical component force of the tilling resistance of the soil to the rotary blade roller, 246 N.

The balance equation of the vibration dynamic system is shown in equation (6):

$$\begin{cases} m_1\ddot{x}_1 = F - k_1\left[x_1 - (x_4 - a\tan\theta)\right] \\ m_2\ddot{x}_2 = -k_2\left[x_2 - (x_4 + b\tan\theta)\right] \\ m_3\ddot{x}_3 = -k_3\left[x_3 - (x_4 + c\tan\theta)\right] \\ m_4\ddot{x}_4 = k_1\left[x_1 - (x_4 - a\tan\theta)\right] + k_2\left[x_2 - (x_4 + b\tan\theta)\right] \\ \quad + k_3\left[x_3 - (x_4 + c\tan\theta)\right] - k_4\left[(x_4 + d\tan\theta) - x_5\right] \\ m_5\ddot{x}_5 = k_4\left[(x_4 + d\tan\theta) - x_5\right] - Q_y - k_5 x_5 - c_1\dot{x}_5 \\ J\ddot{\theta} = bk_2\left[x_2 - (x_4 + b\tan\theta)\right] + ck_3\left[x_3 - (x_4 + c\tan\theta)\right] \\ \quad - ak_1\left[x_1 - (x_4 - a\tan\theta)\right] - dk_4\left[(x_4 + d\tan\theta) - x_5\right] \end{cases} \tag{6}$$

Where:

J is the rotational inertia of the frame rotation around its centroid, [kg·m^2].

Based on equation (6), the vibration simulation program of the tiller was constructed, as shown in fig.11.
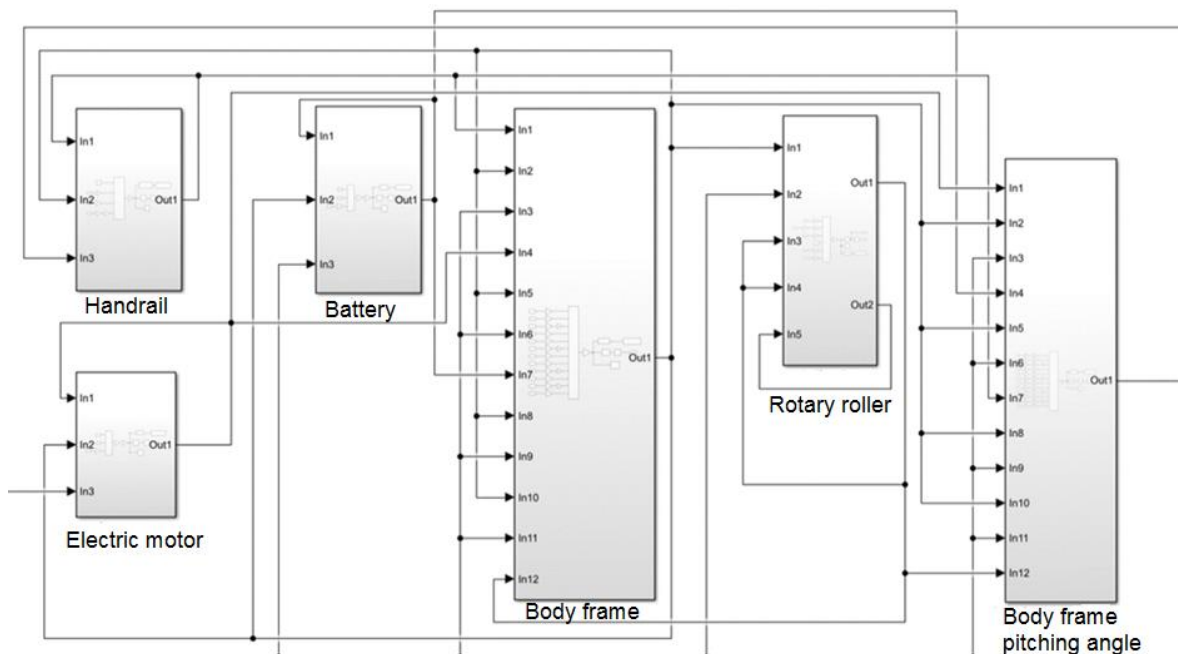

Fig. 12 - Vibration simulation program of the tiller in Simulink

The relevant parameter values (table 10) obtained from 2.2.2 and 2.2.3 were input into the vibration simulation program of the tiller.

Table 10

Parameter values in the balance equation of the vibration dynamic system

Parameter	Value	Parameter	Value
F [N]	154.24	b [m]	0.061
Q_y [N]	246	c [m]	0.242
m_1 [kg]	3.21	d [m]	0.093
m_2 [kg]	6.59	k_1 [N/m]	5.5×10^7
m_3 [kg]	8.38	k_2 [N/m]	5.5×10^7
m_4 [kg]	13.32	k_3 [N/m]	5.5×10^7
m_5 [kg]	12.44	k_4 [N/m]	5.5×10^7
J [kg·m^2]	240	k_5 [N/m]	4.5×10^6
a [m]	0.378	c_1 [N·s/m]	4.5×10^3

The system simulation time was set to 10 s.

RESULTS

Comparison of RMS values obtained by simulation analysis and field test

The vibration acceleration curves and RMS values in *X* direction obtained by the field test and simulation analysis are shown in figs.12 and13, respectively, as well as table 11.
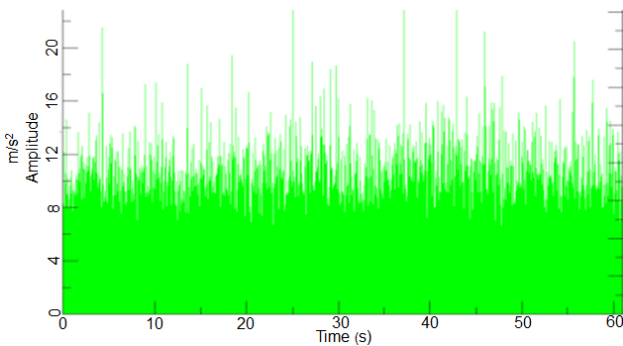

Fig.12 - Vibration acceleration curve from the field test
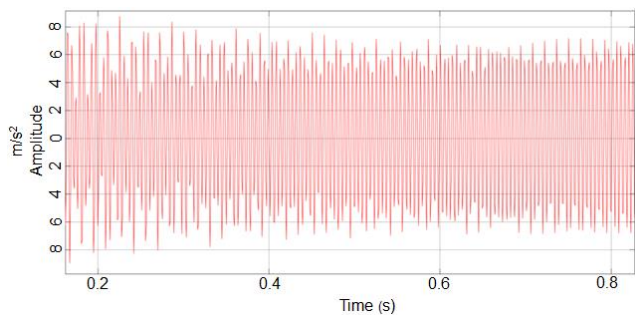
Fig.13 - Vibration acceleration curve from the simulation analysis

Table 11

RMS values

Position	Field test	Simulation analysis	Relative error
	[m/s²]	[m/s²]	[%]
Handle	8.12	7.69	5.30

As seen from Table 11, the RMS values obtained by the simulation analysis were in good agreement with those from the field test (relative error of 5.3%). Therefore, simulation analysis can be used to analyse and improve the operating comfort of the electric mini-tiller.

Centre of gravity adjustment

For the electric tiller, the electric motor and rotary blade roller are installed on its frame by bolts and pins, respectively, and are directly connected with the transmission system, making position adjustment relatively difficult. However, the battery pack is placed on the frame and fixed with elastic rope, which is easy to assemble and disassemble, as well as reposition. Therefore, the position of the battery pack was adjusted to change the position of the centre of gravity.

According to equation (5), when the centre of gravity of the tiller is moved 19.78 cm toward the handrail, and its horizontal distance to the origin increases from 3.52 cm to 23.3 cm, the vertical force at the handles attains its minimum value of 0 N. In order to meet this centre of gravity adjustment requirement, the battery pack was shifted 39.6 cm toward the handrail, to a position between the electric motor and the handrail.

After the centre of gravity adjustment, the three-dimensional model of the tiller was established (fig.14) with point C' (-23.3 cm, 20.616 cm, and -0.042 cm). The vibration dynamic model was then constructed (fig.15), with a balance equation and vibration simulation program identical to those used before the centre of gravity adjustment.


Fig.14 - Three-dimensional model
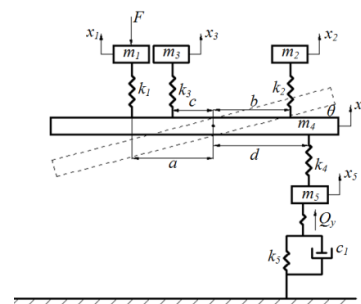
Fig.15 - Vibration dynamic model

The vertical force at the handle F is 0 N, a, b, c, and d are 0.180 m, 0.532 m, 0.154 m, and 0.615 m, respectively. The remaining parameter values are the same as those before the centre of gravity adjustment.

Vibration comparison before and after the centre of gravity adjustment

The RMS values at the handles were obtained by inputting the parameter values after the centre of gravity adjustment into the vibration simulation program of the tiller.

The RMS values before and after the centre of gravity adjustment are listed in table 12.

Table 12

RMS values before and after the centre of gravity adjustment

Position	Before adjustment	After adjustment	Reduction rate
	[m/s^2]	[m/s^2]	[%]
Handle	7.69	6.14	20.16

From table 12, it can be seen that the RMS value at the handles decreased by 20.16% compared with the value before the centre of gravity adjustment, from 7.69 m/s^2 to 6.14 m/s^2.

CONCLUSIONS

1) The RMS values obtained by the simulation analysis were in good agreement with those from the field test (relative error of 5.3%). Therefore, simulation analysis can be used to analyse and improve the operating comfort of the electric mini-tiller.

2) According to the relationship between the centre of gravity and the vertical force at the handles, when the centre of gravity of the tiller was shifted 19.78 cm toward the handrail, and the horizontal distance of the centre of gravity to the origin increased from 3.52 cm to 23.3 cm, the vertical force decreased from 154.24 N to 0 N.

3) Based on the requirement of the centre of gravity adjustment, the layout of the electric mini-tiller was adjusted by shifting the position of the battery pack 39.6 cm toward the handrail, to a position between the electric motor and the handrail. The RMS value then decreased by 20.16%, compared with the value before the centre of gravity adjustment, from 7.81 m/s^2 to 6.14 m/s^2.

4) After the centre of gravity adjustment, when the electric mini-tiller progresses at a forward speed of 0.5 m/s, both the vertical force and the vibration at the handles are reduced, thereby improving operating comfort.

REFERENCES

[1] Asl J.H., Singh S., (2009), Optimization and evaluation of rotary tiller blades: Computer solution of mathematical relations. *Soil & Tillage Research*, vol.106, issue 1, ISSN:0167-1987, pp.1-7, London/U.K.;

[2] Bini, S., Kathirvel K., (2006), Vibration characteristics of walking and riding type power tillers. *Biosystems Engineering*, vol.95, issue 12, ISSN:1537-5110, pp.517-528, London/U.K.;

[3] Caffaro F., Cremasco M.M., Preti C. et al., (2016), Ergonomic analysis of the effects of a telehandler's active suspended cab on whole body vibration level and operator comfort. *International Journal of Industrial Ergonomics*, vol.53, ISSN:0619-8141, pp.19-26, London/U.K.;

[4] Cai K., Zhang J.L., Ke X.R. et al., (2013), Research on the control system of dual-driven electric rotary tiller (两轮独立驱动电动微耕机的控制系统研究). *Guangdong Agricultural Sciences*, vol.40, issue 14, ISSN:1004-874X, pp.179-181, Guangzhou/China;

[5] Gao H.S., Zhang S.H., Shi J.L. et al., (2012), Development of electric micro-farming machines for green-houses (温室大棚用电动微耕机研制). *Journal of Machine Design*, vol.29, issue 11, ISSN:1001-2354, pp.83-87, Beijing/China;

[6] Chen J., Chen C., Chen H., (2014), Three new challenges micro tillers face in southwest China and study of countermeasures. *Journal of Agricultural Mechanization Research*, vol.36, issue 10, ISSN:1003-188X, pp.245-248, Haerbin/China;

[7]   Dong X.Q., Song J.N., Wang J.C. et al., (2012), Vibration frequencies optimization and movement characteristics analysis of vibration shovel for meadow (草地振动松土机运动特性分析与振动频率优化). *Transactions of the Chinese Society of Agricultural Engineering,* ISSN:1002-6819, vol.28, issue 12, pp.44-49, Beijing/China;

[8]   Hu C.J., (2018), Structural Optimization Design and Vibration Analysis of Electric Mini-tiller (电动微耕机整机结构优化设计及振动分析). *Master Dissertation of Southwest University,* Chongqing/China;

[9]   ISO Copyright Office, (2001), *ISO 5349-a. Mechanical vibration-measurement and evaluation of human exposure to hand transmitted vibration, part 1: general requirements*, Geneva, Switzerland;

[10]   Li G., Chen J., Xie H.J. et al., (2016), Vibration test and analysis of mini-tiller. *International Journal of Agricultural and Biological Engineering*, vol.9, issue 3, ISSN:1394-6344, pp.97-10, Beijing/China;

[11]   Liang X.C., Chen J., Wang Z., (2018), Research on the vibration of mini-tiller. *INMATEH-Agricultural Engineering*, vol.56, issue 3, ISSN:2068-4215, pp.17-24, Bucharest/Romania;

[12]   Niu P., Yang M.J., Chen J. et al., (2017), Structural optimization of handrail of a handheld tiller by vibration modal analysis. *INMATEH-Agricultural Engineering*, vol.52, issue 2, ISSN:2068-4215, pp.91-98, Bucharest/Romania;

[13]   Ragni L., Vassalini G., Xu F. et al., (1999), Vibration and noise of small implements for soil tillage. *Journal of Agricultural Engineering Researches*, vol.74, issue 4, ISSN:0021-8643, pp.403-409, London/U.K.;

[14]   Servadio P., Marsili A., Belfiore N.P., (2007), Analysis of driving seat vibrations in high forward speed tractors. *Biosystems Engineering*, vol.97, issue 2, ISSN:1537-5110, pp.171-180, London/U.K.;

[15]   Tewari V.K., Dewangan K.N., (2009). Effect of vibration isolators in reduction of work stress during field operation of hand tractor. *Biosystems Engineering*, vol.103, issue 4, ISSN:1537-5110, pp.146-158, London/U.K.;

[16]   Thomas H.L., Morten K.E., Ario K., (2015), Experimental analysis of occupational whole-body vibration exposure of agricultural tractor with large square baler. *International Journal of Industrial Ergonomics*, vol.47, issue 5, ISSN:0619-8141, pp.79-83, London/U.K.;

[17]   Xu L.Z., Li Y.M., Sun P.P. et al., (2014), Vibration measurement and analysis of tracked-whole feeding rice combine harvester (履带式全喂入水稻联合收获机振动测试与分析). *Transactions of the Chinese Society of Agricultural Engineering,* vol.30, issue 8, ISSN:1002-6819, pp.49-55, Beijing/China;

[18]   Ying Y.B., Zhang L.B., Dong M.D. et al., (1994), Study on absorber of vibration transmitted by walking tractor handles (手扶拖拉机手把减振装置的研究). *Transactions of the Chinese Society of Agricultural Engineering,* vol.10, issue 4, ISSN:1002-6819, pp.74-79, Beijing/China;

[19]   Zhao R.H., Wu Y.Q., Liu Z.Z. et al., (2015), Design of electric micro rotary tiller (温室电动微耕机的设). *Shandong Agricultural Sciences*, vol.47, issue 2, ISSN:1001-4942, pp.129-131, Jinan/China.